Non-invasive peptides delivery using chitosan nanoparticles assembled via scalable microfluidic technology

Giorgia Maurizii , Sofia Moroni , Javier Vicente Jimènez Núnez , Giulia Curzi , Mattia Tiboni , Annalisa Aluigi , Luca Casettari

PII: S2666-8939(24)00004-5
DOI: https://doi.org/10.1016/j.carpta.2024.100424
Reference: CARPTA 100424

To appear in: *Carbohydrate Polymer Technologies and Applications*

Received date: 22 September 2023
Revised date: 3 January 2024
Accepted date: 5 January 2024

Please cite this article as: Giorgia Maurizii , Sofia Moroni , Javier Vicente Jimènez Núnez , Giulia Curzi , Mattia Tiboni , Annalisa Aluigi , Luca Casettari , Non-invasive peptides delivery using chitosan nanoparticles assembled via scalable microfluidic technology, *Carbohydrate Polymer Technologies and Applications* (2024), doi: https://doi.org/10.1016/j.carpta.2024.100424

Non-invasive peptides delivery using chitosan nanoparticles assembled via scalable microfluidic technology

Giorgia Maurizii[1], Sofia Moroni[1], Javier Vicente Jimènez Núnez[1], Giulia Curzi[2], Mattia Tiboni[1], Annalisa Aluigi[1] and Luca Casettari[1,2*]

[1]*Department of Biomolecular Sciences, University of Urbino Carlo Bo, Piazza del Rinascimento, 6, 61029 Urbino (PU), Italy.*

[2]*Prosopika srl, Via Fano, 1/1, 61036 Colli al Metauro (PU), Italy*

Abstract

The delivery of peptides via non-invasive administration routes remains a challenge to be addressed. In this regard, chitosan nanoparticles (CS NPs) have shown promise. However, their current batch preparation methods (ionotropic gelation, polyelectrolyte complexing, emulsification solvent diffusion or micro emulsification) have proven difficult to scale up. Here, we established a microfluidic-assisted ionotropic gelation method for the manufacturing of CS NPs, ionically crosslinked with sodium tripolyphosphate (TPP), and loaded with a model peptide, Argireline. The microfluidic process was optimized through a design of experiments approach. CS concentration and pH have the greatest effect on particle size, while CS and TPP concentrations and pH on PDI. The optimum formulation was successfully loaded with the peptide (90% EE) and characterized by a size of 186.0 ± 1.0 nm and a PDI of 0.440 ± 0.002. Subsequently, Argireline-loaded CS-TPP NPs suspension was converted into a gel for a potential topical application, considering the non-toxic, biocompatible, and biodegradable properties of the components used in the formulation. The NPs gel demonstrated appropriate mechanical properties for Argireline transdermal delivery, along with improved control over its release and enhanced skin permeation for up to 48 hours, compared to NPs suspension and free drug solution. Hence, this study demonstrated that the microfluidic-assisted ionotropic gelation method could be an easy-scalable platform for the manufacturing of peptide-loaded CS-TPP NPs which could be potentially applied for the transdermal delivery of biologics.

Keywords: Chitosan; Peptide; Microfluidic; Design of Experiment; Drug delivery systems

1. Introduction

Recently, peptide therapeutics have emerged in the pharmaceutical market as an alternative to conventional small-molecule drugs (Pagels et al., 2015). The high selectivity, potency, and low toxicity make peptides propitious drugs for treating several diseases. However, the increased clinical use of these biologics highlighted some pharmacokinetic limitations that have led to their exclusive use as injectable formulations (Agrahari et al., 2016, Patel et al., 2014). Indeed, the high molecular weight, limited membrane permeability, chemical/enzymatic instability, and immunogenicity of peptides pose substantial challenges in developing non-invasive drug delivery systems (Bajracharya et al., 2019). Consequently, appropriate formulation strategies are needed to achieve efficient peptide administration via non-invasive routes (e.g., oral, nasal, pulmonary, and transdermal).

Among these strategies, polymeric nanoparticle-based delivery systems (PNPs) are particularly promising. PNPs are organic-based NPs (size range from 1 to 1000 nm) in which the loaded active compound is entrapped within or surface-adsorbed onto the polymeric core (Zielińska et al., 2020). PNPs offer numerous benefits in loading biologics as cargos, such as protection against premature degradation, bioavailability, retention time, targeted delivery, and improvement of intracellular penetration (Kumari et al., 2010, Yan et al., 2020).

Chitosan has gained an outstanding position in manufacturing PNPs, as a biodegradable, biocompatible, and mucoadhesive polymer (Mikušová et al., 2021), together with its antimicrobial and antioxidant properties (Campana et al., 2017, Casettari et al., 2012). Commonly, chitosan nanoparticles (CS NPs) are prepared via ionotropic gelation, a simple, low-cost, and eco-friendly process, which is based on ionic crosslinking between positive amino groups of CS and negatively charged small molecules like pentasodium tripolyphosphate (TPP) (Hashad et al., 2016, Farahani et al., 2021). Indeed, the ionotropic gelation phenomenon exploits the capacity of polyelectrolytes, such as polysaccharides, to react with molecules that have opposite charges, and undergo the sol-gel transition, which forms structured physical materials (e.g., nanoparticles) (Gadziński et al., 2022). The ionotropic gelation method can be performed through different techniques. In this context, microfluidic technology has proven to be one of the most effective tools to overcome typical drawbacks, such as batch-to-batch variability and low production rate, related to conventional bulk mixing methods (Greco et al., 2023, Soheili et al., 2021).

Microfluidics enables the manipulation of nanoliters scale of fluids in micron-sized channels within a microfluidic chip. The in-flow process and miniaturization of the reaction environment allow accurate control over the NPs' physiochemical properties (e.g., size and polydispersity index (PDI)), improving batch-to-batch reliability. Moreover, the formulation can be optimized at small volumes, by varying microfluidic parameters (e.g., total flow rate (TFR) and flow rate ratio (FRR)) and internal geometries of the chip. In this way, the NPs synthesis can be easily scaled up in a cost- and time-saving manner (Hickey et al., 2015, Chiesa et al., 2020, Chiesa et al., 2021, Sommonte et al., 2023).

In this study, a 3D-printed custom-made microfluidic chip was used to prepare CS-TPP NPs loaded with Argireline, as model peptide, by exploiting the ionotropic gelation method. The main aim was to develop a reproducible microfluidic manufacturing method of CS-TPP NPs which allows efficient encapsulation and appropriate delivery of peptides. Preparation conditions of drug-free CS-TPP NPs were optimized with a Design of Experiment (DoE) approach, by varying the flow rate, pH, and concentrations of the polyelectrolyte streams, and characterizing the nanoparticles concerning size and PDI. Optimized drug-free and loaded CS-TPP NPs were characterized by their average particle size, PDI, encapsulation efficiency (EE%), and stability, and their chemical composition and thermal behavior were investigated by Fourier-transformed infrared spectroscopy (FTIR) and thermogravimetric analysis (TGA) respectively. Moreover, in view of a potential topical application, we used optimized Argireline-loaded CS-TPP NPs to prepare a gel with enhanced retention time at the skin surface to facilitate the peptide delivery. The in vitro Argireline release and permeation profiles of both nanoparticles and gel formulations were determined with vertical diffusion cells and compared, and the mechanical and rheological properties of the gel were also assessed.

2. Materials and Methods

2.1 Materials

Chitosan HCl (Chitoceuticals) with a degree of deacetylation of 82.2 % and a viscosity of 19 mPas (1 % in water, 20 ºC), and an approximate molecular weight of ~300 kDa was purchased by Heppe Medical Chitosan GMBH (HMC+) (Halle, Germany). Sodium Tripolyphosphate was purchased by Sigma-Aldrich (Sant Louis, USA). Carboxymethylcellulose sodium was provided by Galeno (Prato, Italy). Argireline was kindly donated by Lipotec^{TM} Active Ingredients (Wickliffe, Ohio, USA). All the reagents used were around 96-98% pure. All the solvents used were analytical grade.

2.2 3D printing of microfluidic chips

The design and printing of the 3D-printed chips were done as previously mentioned (Tiboni et al., 2021). A computer-aided design (CAD) was used to optimize the microfluidic chip's architecture and achieve an efficient passive micromixing with “split and recombine’’ channels (C-chip). The devices were then printed using polypropylene filament with a fused deposition modeling (FDM) 3D printer (Ultimaker 3, Ultimaker, The Netherlands) at a print speed of 25 mm/s and with a nozzle temperature of 220 °C (0.25 mm nozzle). Finally, probe needles were utilized to link, through polyethylene tubing, the 3D-printed chip to two syringes mounted on two syringe pumps (Aladdin, WPI Europe, Germany).

2.3 Microfluidic formulation of drug-free nanoparticles (NPs)

For the preparation of drug-free NPs (CSTPP@NPs) by microfluidics, a defined amount of chitosan (CS) was dissolved into a solution of acetic acid (1% v/v) in water. Three different final CS concentrations were evaluated, *i.e.,* 2, 2.5, and 3 mg. The pH of this phase was adjusted using sodium hydroxide 3M until reaching the desired pH of 3, 4, or 5. Meanwhile, a solution of sodium tripolyphosphate (TPP) in water was prepared, taking into account three different final TPP concentrations, *i.e*. 0.4, 0.5, and 0.6 mg/ml. The two phases were then mixed through the microfluidic device (Figure 1) with a FRR 1:1 and different TFR of 4, 8 and 12 ml/ml. Finally, the flow-out NPs were collected from the chip's outlet.

A Design of Experiment approach (DoE) was used to evaluate the main effects of the process parameters (independent variables) such as CS concentration, TPP concentration, pH, and TFR, as well as their interactions on the particle size and PDI (dependent variables). The Box-Behnken design was used to define the numbers and kinds of experiments (Table 1); while the ANOVA analysis was performed to define and validate the multiple regression mathematical model. To this end a statistically significant level of 5 % was considered and regression coefficients R^2, adjusted-R^2 (adj-R^2), and predicted R^2 (pred-R^2) were discussed. The R^2 coefficient is a measure of how well a regression model predicts an outcome. However, R^2 always increases when new terms are added to the regression model, even if they are not significant (overfitting). The modified adj-R^2 is a modified version of R^2, which increases only if the new term of the models improves the fitting of the experimental data; otherwise, it decreases. Therefore, the adj-R^2 allows the comparison of regression models differing by the number of terms. The pred-R^2 indicates how well a regression model makes predictions. The adj-R^2 and pred-R^2 have to be in good agreement (i.e. their difference must be less than 0.2). Matlab 2022Rb and OriginPro software were used to create the DoE and to elaborate the results.

Table 1. *Optimization of the microfluidic manufacturing process of CSTPP@NPs by the design of experiment (DoE): size and polydispersity index (PDI) of the different batches (Run (No.) 1–27).*

	INPUT				**OUTPUT**	
RUN	**pH**	**CS concentration (mg/mL)**	**TPP Concentration (mg/mL)**	**TFR**	**Size (nm)**	**PDI**
	X_1	X_2	X_3	X_4	Y_1	Y_2
1	5	2.5	0.5	12	97	0.24
2	5	2	0.5	8	75	0.20
3	5	2.5	0.6	8	90	0.22
4	5	2.5	0.4	8	92	0.26
5	5	3	0.5	8	108	0.31

6	5	2.5	0.5	4	106	0.26
7	4	3	0.5	4	129	0.47
8	4	2.5	0.4	4	100	0.34
9	4	2	0.4	8	76	0.36
10	4	2	0.5	4	102	0.31
11	4	2.5	0.5	8	100	0.44
12	4	3	0.4	8	99	0.45
13	4	2.5	0.6	4	100	0.29
14	4	3	0.5	12	102	0.40
15	4	2	0.6	8	79	0.26
16	4	3	0.6	8	92	0.38
17	4	2.5	0.5	8	87	0.30
18	4	2.5	0.4	12	81	0.34
19	4	2.5	0.5	8	86	0.33
20	4	2	0.5	12	76	0.28
21	4	2.5	0.6	12	80	0.32
22	3	2.5	0.4	8	131	0.64
23	3	3	0.5	8	119	0.42
24	3	2.5	0.5	4	121	0.43
25	3	2.5	0.6	8	115	0.42
26	3	2.5	0.5	12	111	0.42
27	3	2	0.5	8	98	0.42

2.4 Microfluidic formulation of Argireline-loaded nanoparticles (NPs)

To obtain Argireline-loaded NPs (Arg@NPs), the drug was dissolved in the CS solution with a weight ratio (Argireline/CS) of 2:1. The rest of the process was performed by using the conditions of run 2 (Table 1) which are a CS concentration of 2 mg/mL, a TPP concentration of 0.5 mg/mL, a pH of 5 and a TFR of 8 mL/min.

2.5 Physicochemical characterization of NPs

2.5.1 Dynamic Light Scattering (DLS)

Prepared formulations were investigated by measuring their average particle size (Z-average) and polydispersity index (PDI) with a Malvern Zetasizer Nano S instrument (Malvern Instrument Ltd, UK). The

concentration of the prepared nanoparticles was 1 mg/ml. Prior to the measurements, the formulations were diluted at 1:10 in distilled water to obtain a final nanoparticles concentration of 0.1 mg/ml. Stability tests were performed on all formulations (Table 1) by storing them at 4 °C for 30 days and measuring their size after 7 and 30 days of production.

2.5.2 Nanoparticles Tracking Analysis (NTA)

To further characterize the NPs, Nanoparticles Tracking Analysis (NTA) measurements were performed by using a NanoSight LM10 instrument (NanoSight, Malvern, UK). Before the test, all the samples were serially diluted with a Phosphate Buffer Saline solution (PBS at pH=7.4) to reach a particle concentration suitable for analysis with NTA. After that, each sample was injected into the LM unit with a 1 ml sterile syringe, and five 60-second videos were recorded and then analyzed with the Nanoparticle Tracking Analysis (NTA) 3.1 Analytical software (Nanosight, Malvern, UK). Data are presented as the mean ± SD of the five video recordings.

2.5.3 Environmental Scanning Electron Microscopy (ESEM)

An environmental scanning electron microscope (ESEM) (FEI, Hillsboro, OR, USA) was used to investigate the surface morphology of the Arg@NPs. For ESEM analysis, the instrument was utilized in low-vacuum mode, with a specimen chamber pressure set from 0.6 to 0.80 mbar, an accelerating voltage of 25 kV, a working distance of 10.4 mm, and a magnification ranging between 8000 and 165000×. The images were obtained using a secondary electron detector.

2.5.4 Fourier Transformed Infrared Spectroscopy (FT-IR)

FT-IR spectra of pure TPP, CS, Argireline, and the selected CSTPP@NPs (run 2, Table 1) and Arg@NPs formulations were taken with FTIR spectrophotometer (ATR-FTIR, Spectrum Two FT-IR spectrometer with ATR accessory, Perkin Elmer, MA, USA) with the resolution of 4 cm^{-1} in the range of 450–4000 cm^{-1}. Prior to analysis NPs samples were frozen at -20 °C, and, the following day, freeze-dried for 24 h using an Edwards Modulyo freeze dryer (Edwards, Burgess Hill, UK).

2.5.5 Thermogravimetric Analysis (TGA)

The thermal stability of raw materials and selected CSTPP@NPs and Arg@NPs were investigated through thermogravimetric analysis (TGA 4000, Perkin Elmer, USA). TGA was performed in the range of 30 to 600 °C at a heating rate of 10 °C/min under a nitrogen flow rate of 30 mL/min. TGA tests were carried out on freeze-dried nanoparticles. Pyris Manager software (Perkin Elmer, USA) was used for data collection and analysis.

2.5.6 Encapsulation Efficiency (EE %) studies

Encapsulation Efficiency (EE %) studies were carried out using the indirect method. A precise amount of Argireline-loaded NPs was ultracentrifuged at 17.200 RCF at room temperature for 30 minutes. Thereafter, the amount of unloaded Argireline was measured in the supernatant of the preparation medium using high-performance liquid chromatography (HPLC, Agilent 1260 Infinity II, Agilent, USA). Before the analyses, a calibration curve of Argireline standard was performed with several concentrations in the range of 0.001 to 1 mg/mL with a correlation coefficient (R^2) of 0.9987.

The EE % of Argireline was calculated with the following equation (Eq. 1):

$$EE\ \% = \frac{T_{drug} - S_{drug}}{T_{drug}} \quad \text{(Eq. 1)}$$

where T_{drug} is the total amount of drug used for the formulation and S_{drug} is the amount of drug in the supernatant measured with HPLC.

2.6 Arg@NPs gel preparation

The Arg@NPs formulation was pre-treated to remove the non-encapsulated active compound. Specifically, 10 mL of sample were placed into a dialysis bag (MW cut off 12 k-14 k Da, Spectra/Por™, Spectrum Labs, USA) immersed into 2 L of a solution of acetic acid (1 % v/v) in water for 30 minutes, under stirring, at room temperature. The purified NPs suspension was then converted into a gel by adding sodium carboxymethylcellulose (5 % w/v) upon continuous and gentle stirring. The prepared gel was kept at room temperature overnight for complete polymer hydration.

2.7 Gel characterization

2.7.1 pH evaluation

1 g of the Arg@NPs-based gel was dissolved in 25 ml of distilled water and the resulting solution was used to measure the pH using a digital pH meter (HI2211-02 Basic pH/ORP Benchtop Meter, Hanna Instruments, USA) (Singh et al., 2019). Experiments were performed in triplicate and average pH values were calculated.

2.7.2 Rheological measurements

Rheological measurements of Arg@NPs gel were carried out using a coaxial rotation viscometer (RheolabQC, Anton Paar, Austria) with a cylinder-in-cylinder type measuring geometry. The rheological characteristics were determined in the range of shear rates from 1 to 100 s^{-1}. Tests were performed in triplicate.

2.7.3 Texture Profile Analysis (TPA)

Textural measurements were performed with a TA.XT plus Texture Analyzer (Stable Micro Systems, UK) which was set in compression mode. About 40 g of the Arg@NPs gel was placed approximately one inch

below the instrument's 18 mm cylindrical probe. In each test, the probe was initially lowered to the surface of the sample at a pre-test speed of 1 mm/s until reaching contact. Contact was detected by a triggering force of 0.049 N, and then the probe produced an additional 8 mm deformation of the sample at a test speed of 2 mm/s before rising to the calibration height (at a post-test speed of 2 mm/s). After 5 s, the measurement cycle was repeated on the same sample. Six replicate analyses were performed at room temperature using a fresh sample in each case. The resulting force-time curve was used to calculate some mechanical parameters, such as hardness, compressibility, adhesiveness, and cohesiveness (Carvalho et al., 2012, Tai et al., 2014).

2.7.4 Drug content

100 mg of the Arg@NPs-based gel was dissolved in 20 ml of phosphate buffer saline solution (PBS at pH 7.4) under magnetic stirring. The solution was then filtered using Whatman filter paper no.1 and the filtered solution was analyzed with HPLC (HPLC Agilent 1260 Infinity II, Agilent, USA) (Singh et al., 2019).

2.8 HPLC method for the quantitative analysis of Argireline

The amount of Argireline released from NPS was evaluated by high-performance liquid chromatography (HPLC Agilent 1260 Infinity II, Agilent, USA). The mobile phase consisted of a mixture of 0.05 % of TFA in water and ACN and a gradient elution method (Table 2) with a flow rate of 0.5 mL/min was used. The injection volume was 5µL in an Agilent Poroshell 120 EC-C18, 100 × 4.6 mm, 2.7 µm column (Agilent, USA), and the detection signal was recorded at 215 nm, keeping the analysis system at room temperature.

Table 2. *Gradient elution program for HPLC analysis.*

Time (min)	A% (H_2O + 0.05 % TFA)	B% (ACN + 0.05 % TFA)
0.00	95	5
15.00	45	55
15.10	95	5
20.00	95	5

2.9 In vitro release and permeation studies using Franz-type diffusion cells

To perform the release and permeation studies the Arg@NPs formulation was pre-treated as described in section 2.6. The *in vitro* release and permeation profiles of Argireline from Arg@NPs and Arg@NPs gel were evaluated using Franz-type diffusion cells with a receptor compartment volume of 7 mL and an effective diffusion area of 1.766 cm^2. PBS (pH= 7.4) was used as receptor media and the receptor compartment was stirred continuously at 400 rpm by a magnetic stirrer. The system was thermostated at 32 ± 0.5 °C with a circulating jacket. A dialysis membrane (MW cut off 12 k-14 k Da, Spectra/Por™, Spectrum

Labs, USA) and a Strat-M® membrane (Merck Millipore, USA) were applied as partitioning membranes for the *in vitro* drug release study and *in vitro* permeation study respectively. At predetermined sampling intervals (1, 2, 4, 6, 8, 24, and 48 hours), samples were withdrawn from the receptor compartment and replaced with an equal volume (0.2 mL) of fresh buffer. The content of Argireline in each sample was then determined by HPLC (HPLC, Agilent 1260 Infinity II, Agilent, USA). Triplicate measurements were made for each sample.

2.10 Mathematical modeling of the kinetics release

To study the release kinetics of Argireline from both Arg@NPs and Arg@NPs gel formulations, the release data were fitted and compared with first-order, Higuchi, Korsmeyer-Peppas, and Peppas-Salhin mathematical models using Origin Software (Origin Pro 2021, OriginLab, USA). The best-fitting model was chosen taking into consideration the adjusted coefficient of determination (adjusted-R^2).

2.11 Stability studies

To investigate the stability of Arg@NPs and Arg@NPs gel, formulations were stored at different temperatures (room temperature and refrigerator temperature) for 1 month and analyzed periodically (0, 15, and 30 days). NPs formulation was evaluated for size, PDI, and EE %, while gel formulation for pH, drug content, and rheological and mechanical properties. All the experiments were performed in triplicate. Statistical significance of the differences between the experimental (Arg@NPs gel, day 0 of storage) and control (Arg@NPs gel, day 15 and 30 of storage at room and refrigerator temperature) groups was assessed via a two-tailed Student's t-test (2-tailed), considering p value <0.05 as a significant result.

3. Results and Discussion

3.1 Optimization of the chitosan nanoparticles manufacturing process by microfluidic

The chitosan nanoparticles ionically crosslinked with TPP (CSTPP@NPs) were successfully prepared by microfluidic technology. Practically, the chitosan nanoparticles were obtained through a continuous mixing process carried out in the C-Chip microchannels (Figure S1) between a chitosan solution and a solution containing the ionic crosslinker TPP, as schematized in Figure 1a. The nanoparticles' formation was induced by the reversible electrostatic interactions between the positively charged chitosan amino groups and the negatively charged tripolyphosphate anions (Figure 1b).

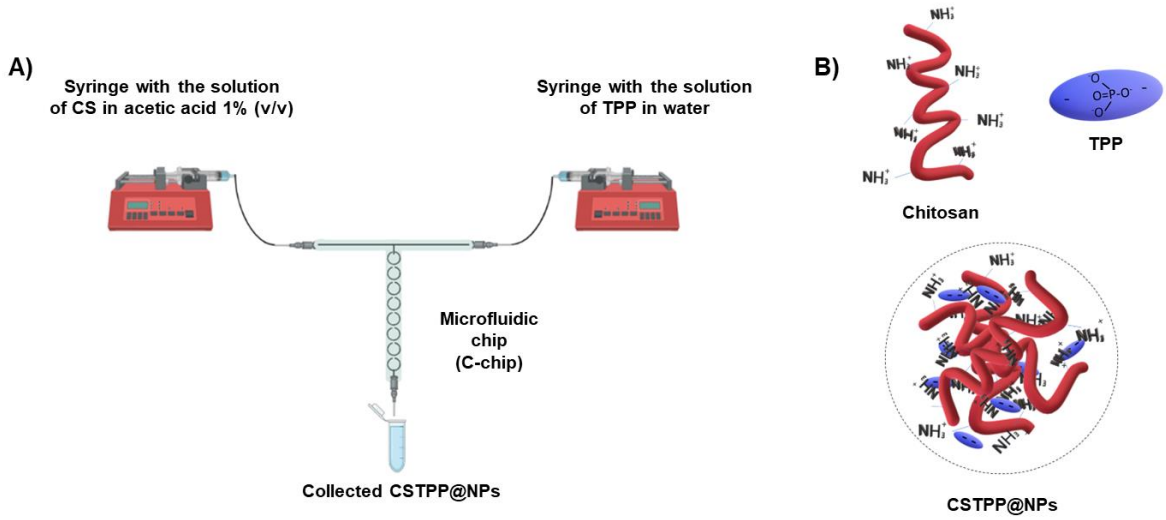

Figure 1. A) *Microfluidic synthesis of CSTPP@NPs;* ***B)*** *Ionic crosslinking between chitosan and TPP.*

To optimize the CSTPP@NPs manufacturing process by microfluidic, a DoE approach was used to understand the effects of pH, chitosan concentration, TPP concentration, and TFR on particle size and PDI. To this end, the responses observed for the 27 runs (Table 1) were first fitted to the quadratic mathematical model (equation 2) whose equation is reported below, and the fit summary for each response is reported in Table 3:

$$Y = \sum_{i=1}^{3} a_i X_i + \sum_{ij=1}^{3} a_{ij} XX_j + \sum_{i=1}^{3} a_{ii} X_i^2 + y_0 \quad \text{(Eq. 2)}$$

After that, the quadratic mathematical model applied for size and PDI was refined by eliminating the insignificant terms of equations (whose p-value > 0.05), as summarized in Table S1.

3.1.1 Effect of input parameters on size (Y_1)

The refined mathematical model for size only includes the linear terms X_1, X_2 and X_4 and the quadratic term X_1^2; while the other terms are not significant. The refined equation (equation 3) for size can be written as follow:

$$Y_1 = 292{,}67 - 110X_1 + 23{,}90X_2 - 2{,}32X_4 + 12{,}44X_1^2 \quad \text{(Eq. 3)}$$

Compared to the quadratic mathematical model, the refined one has a significantly lower *p-value* and a higher Adj-R^2 suggesting that the model can be considered more accurate. Moreover, Pred-R^2 is in good agreement with the Adj-R^2, being their difference lower than 0.2.

Therefore, the particle size is affected by pH, CS concentration, and TFR, while the TPP amount seems to not significantly affect it, in agreement with what was stated by Rázga et al. (Rázga et al., 2016).

Figure 2 shows the 3D response surface plots related to the correlations between particle size and pH and CS concentration (Figure 2a) as well as pH and TFR (Figure 2b). The pH plays a dominant role in determining particle size, since it regulates the electrostatic interactions between the carboxyl groups (COO^-) of TPP and amino groups (NH_3^+) of CS (Rázga et al., 2016). Presumably, the smallest nanoparticles are obtained when a greater number of electrostatic interactions occur between carboxyl groups and protonated amino groups. Nevertheless, with decreasing the pH, the ionization degree of TPP decreases (due to the protonation of COO- groups), while the one of chitosan increases (due to the protonation of NH_2 groups). Therefore, the smallest nanoparticles will be obtained at an optimal intermedium pH value, corresponding to the maximum number of electrostatic interactions. As observed in Figure 2a, the smallest CSTPP@NPs were obtained with an intermedium pH of 4.0-4.5. Moreover, the particle size tends to increase with increasing the CS concentration and with decreasing the TFR.

3.1.2 Effect of input parameters on PDI (Y_2)

The refined mathematical model for PDI, described in the equation 4, only includes the linear terms X_1, X_2 and X_3:

$$Y_2 = 0.734 - 0.105X_1 + 0.101X_2 - 0.428X_3 \quad \text{(Eq. 4)}$$

Also for PDI, compared to the quadratic mathematical model, the refined one has a significantly lower *p-value and a* higher Adj-R^2. Moreover, the Pred-R^2 and the Adj-R^2 are in good agreement (their difference is lower than 0.2), therefore the model can be considered more accurate (Table 3). The PDI is mainly affected by the pH, CS concentration and TPP amount, while the TFR does not influence it.

The 3D response surface plots related to the correlations between PDI and pH and CS concentration, as well as pH and TPP amount are shown in Figure 2c and 2d, respectively. As observed, the PDI decreases with increasing the pH and the TPP concentrations and with decreasing the CS concentration. Indeed, as previously stated, the increased protonation of the CS amino groups takes place at an intermediate pH of 4.0-4.5, allowing for higher interaction with anionic TPP ions. Furthermore, the greater availability of TPP molecules to interact with the free amino groups of CS is the outcome of the elevated TPP concentration. Thus, since cross-linking with TPP reduces the availability of free primary amino groups in chitosan, self-aggregation between the nanoparticles is prevented, resulting in the formation of NPs more homogeneously distributed in size and with lower PDI values (Masarudin et al., 2015).

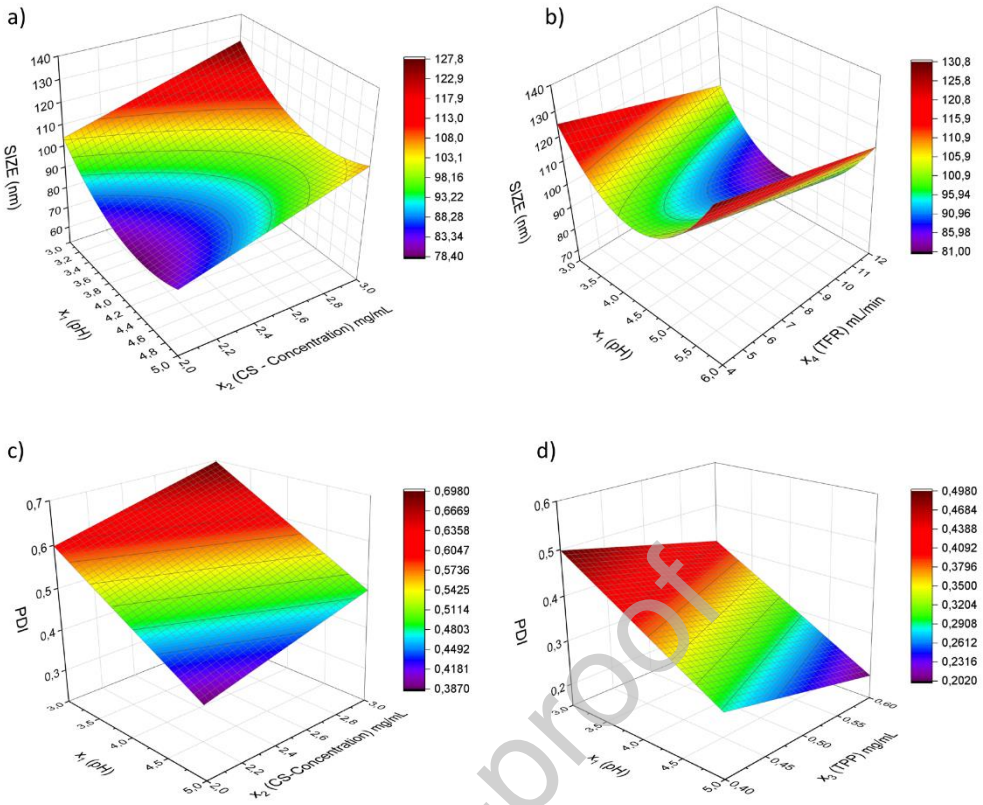

Figure 2. *3D surface plot response of the main effect of a) solution pH and CS concentration, and b) solution pH and TFR on CSTPP@NPs size; and c) solution pH and CS concentration, and d) solution pH and TPP concentration on PDI.*

Table 3. *Analysis of variance (ANOVA) of quadratic and refined models (for size and PDI).*

SIZE (Y_1)/nm			
MODEL	**R^2**	**Adj-R^2**	**Pred-R^2**
Quadratic model (Eq. 1)	0.8539	0.6834	0.2203
Refined model (Eq. 2)	0.7797	0.7396	0.6537
PDI (Y_2)			
MODEL	**R^2**	**Adj-R^2**	**Pred-R^2**
Quadratic model (Eq. 1)	0.8411	0.6557	0.2286
Refined model (Eq. 3)	0.7766	0.7475	0.6839

3.2 Stability of the CSTPP@NPs

Experimental settings of nanoparticles' manufacturing, not only affect their size but also their stability in time (Jonassen et al., 2012). Previous studies reported opposite results regarding the long-term stability of CS-TPP NPs. Some (López-León et al., 2005) illustrated a significant increase in NPs size after 7 days of preparation due to spontaneous aggregation, erosion of particles' spherical shape, hydrolysis of chitosan chains, or swelling. Others (Fan et al., 2012, Morris et al., 2011, Rampino et al., 2013) described no or modest NPs size changes up to one month of storage (Rázga et al., 2016). Similarly, our long-term stability data (Figure 3), based on one month of storage of CSTPP@NPs at 4 °C, displayed only a moderate increase in their size. However, the pH of the CS solution seemed to have a major impact on the size and stability of CSTPP@NPs regardless of the other investigated parameters (CS concentration, TPP concentration, and TFR), since the NPs prepared at pH 5, especially the ones prepared using conditions of run 2, possessed both lower size and higher long-term stability.

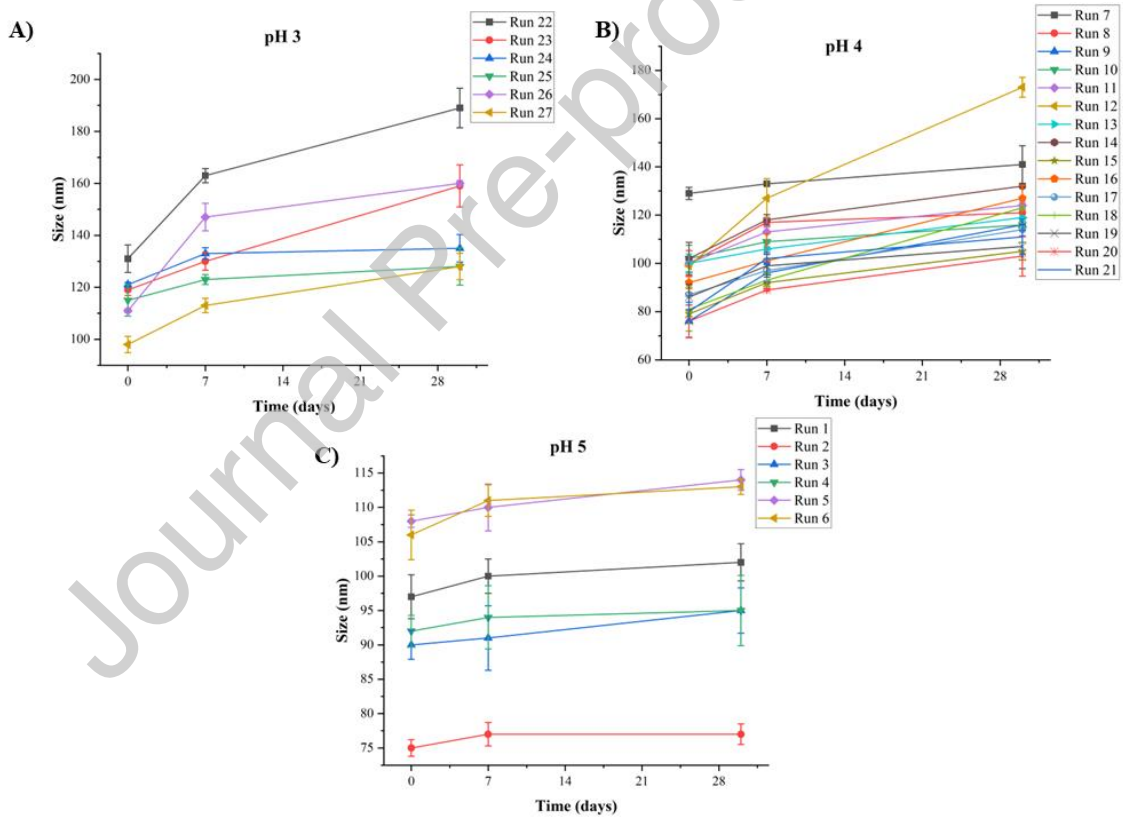

Figure 3. *Long-term stability-to-storage study for CSTPP@NPs prepared at pH 3 (A), 4 (B), and 5 (C), over one month.*

3.3 Characterization of Arg@NPs formulation

3.3.1 Percentage encapsulation efficiency (EE %), particle size, and morphology

Based on the nanoparticles' size and stability, conditions of run 2 (Table 1) were selected to obtain the optimized Argireline-loaded NPs formulation. Moreover, preliminary encapsulation efficiency studies (data not shown) highlighted that the 2:1 weight ratio of Argireline:CS allowed the obtaining of the highest encapsulation of the peptide in the nanoparticles. Effectively, the EE% of the optimized Arg@NPs formulation, investigated by HPLC, was 90.2 % ± 0.7.

Physical characterization of Arg@NPs by DLS showed an average size and PDI of 186.0 ± 1.0 nm and 0.440 ± 0.002 respectively. Instead, the average size distribution of Arg@NPs using the NTA method was 172.5 ± 3.51 nm, and the NPs system exhibited more than one particle population (Figure 4). The difference between the data acquired with DLS and NTA techniques could be due to the several dilutions to which NPs are subjected in the NTA analysis, which may have led to the rupture of aggregates, resulting in smaller average size values, compared to the DLS data (Maruyama et al., 2016). Nevertheless, both analyses revealed a significant increase in the NPs size and PDI after loading with Argireline. This behavior, observed by other authors with other peptides (e.g., bovine serum albumin and human hemoglobin), has been ascribed to the electrostatic interactions between the negatively charged peptide and positively charged chitosan (Rampino et al., 2013). Furthermore, Arg@NPs' concentration calculated from the NTA results was 1.01 x 10^{11} particles/mL.

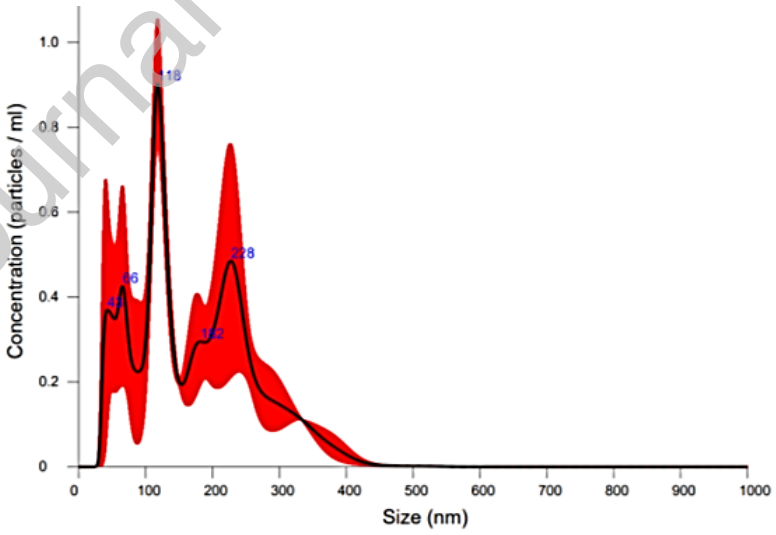

Figure 4. *Calculated mean ± SD of size distribution detected by NTA analysis of Arg@NPs.*

Finally, the surface morphology of the Arg@NPs, after cast drying on an aluminum surface, was observed with an ESEM, as shown in Figure 5. The nanoparticles were fairly smooth and spherical in shape, and the

average size was about 200 nm. However, clusters of the nanoparticles formed probably due to unavoidable aggregation during the drying process (Khoerunnisa et al., 2021).

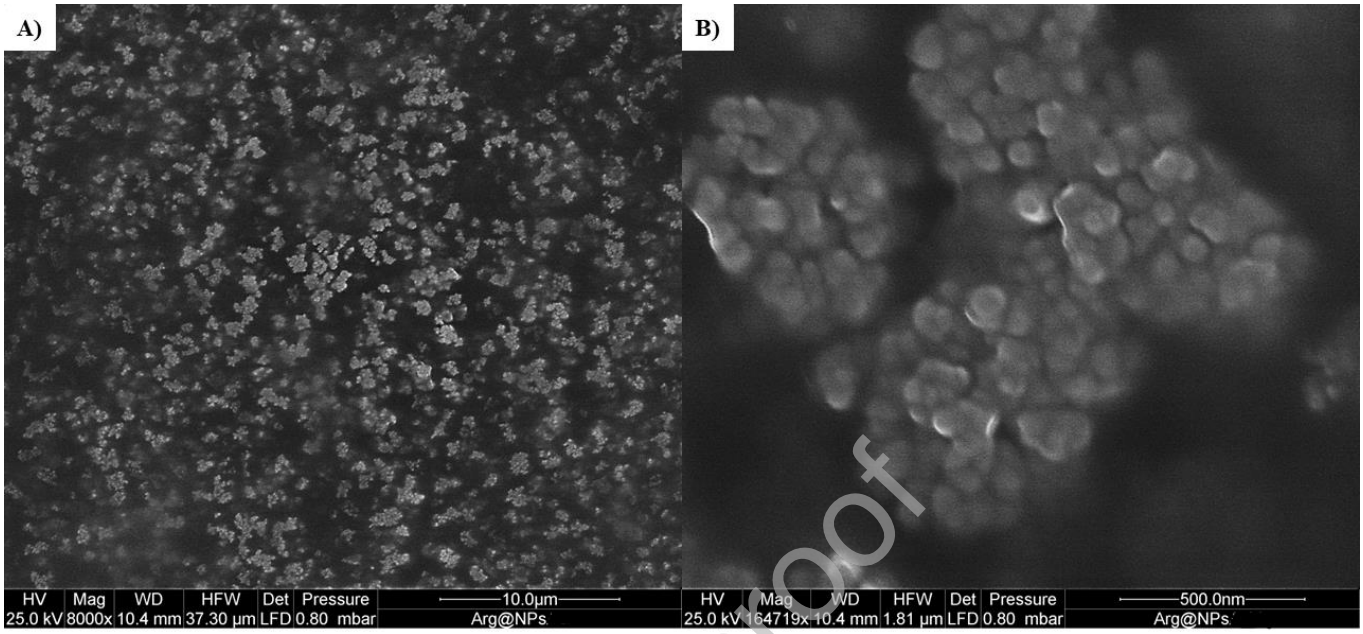

Figure 5. *ESEM images of the synthesized Arg@NPs a) at lower magnification and b) at higher magnification.*

3.3.2 Fourier-Transform Infrared Spectroscopy (FTIR)

FT-IR spectroscopy measurements were performed to thoroughly understand the NPs' formation as well as to study the entrapment of Argireline peptide in CSTPP@NPs. FTIR spectra of CS, TPP, Argireline, CSTPP@NPs, and Arg@NPs, are reported in Figure 6. CS profile shows a strong broad peak at 3325 cm^{-1} which is attributed to -NH_2 and -OH groups stretching vibration, two adsorption bands at 1652 cm^{-1} and 1590 cm^{-1}, which are ascribed to C=O stretching of amide I and to N-H bending of amide II respectively, and adsorption bands at 1080 and 1030 cm^{-1} due to the skeletal vibrations involving O-C bonds. The main vibrations of TPP fall at 1210 cm^{-1} (P=O stretching vibrations), 1130 cm^{-1} (O-P=O stretching vibrations), 1090 cm^{-1} (stretching vibrations of PO_3 groups), and 888 cm^{-1} (asymmetric stretching vibrations of P-O-P groups) (Loutfy et al., 2016). As shown in Figure 6a, a sharper peak at 3325 cm^{1} can be observed in the NPs spectrum, indicating enhanced hydrogen bonding. Moreover, the absorption bands at 1652 cm^{-1} and 1590 cm^{-1} of CS are shifted to 1640 cm^{-1} and 1548 cm^{-1} in NPs because of the electrostatic interactions between NH_3^+ groups of CS and phosphate groups of TPP (Figure 6a). In addition, the significant band at 1411 cm^{-1} observed in the NPs is due to the -CH_2 wagging vibrations, strongly enhanced because of the increased C=O polarization upon interactions (de Carvalho, et al., 2019). Furthermore, the NPs profile exhibits a signal at 1019 cm^{-1} that is indicative of P=O stretching vibrations from phosphate groups (Hosseini et al., 2018, Lustriane et al., 2018).

The Argireline spectrum is characterized by the typical adsorption peaks of peptides such as amide A at 3230 cm^{-1}, amide I at 1637 cm^{-1}, and amide II at 1537 cm^{-1} (Figure 6b). The spectrum of Arg@NPs shows some

differences from CSTPP@NPs in the 1623-1750 cm^{-1} range, which means the formation of peptide-NPs complex (Figure 6b). Specifically, the broadening of the peak related to amide I and its shift to a lower wavenumber probably indicate the electrostatic interactions between the negative charges of peptide fractions and positive charges of CS (Du et al., 2019).

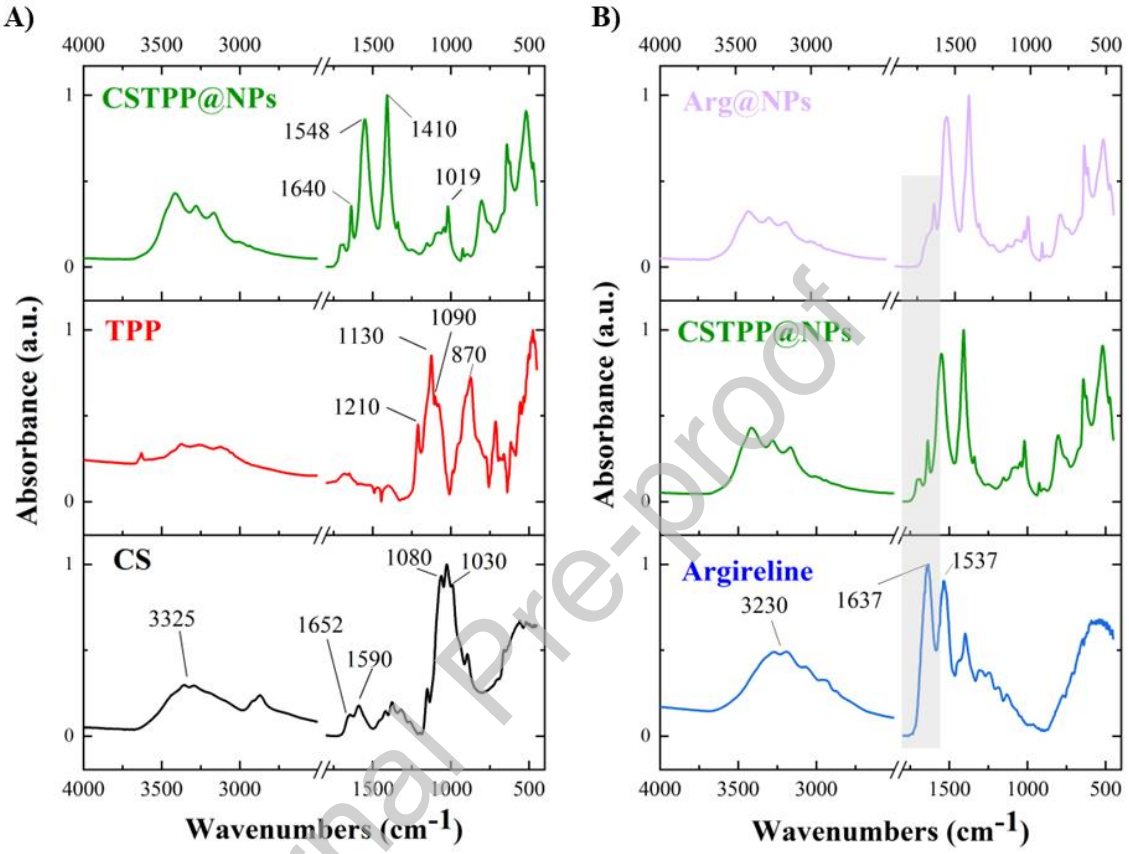

Figure 6. *FT-IR spectra of A) CS, TPP, and CSTPP@NPs, and b) Argireline, CSTPP@NPs, and Arg@NPs.*

3.3.3 Thermal stability

The thermal stability of CS, TPP, Argireline, CSTPP@NPs, and Arg@NPs was investigated by TGA and is given in Figure 7. For CS, the first weight loss (about 9.2 %) occurred at around 30-100 °C and probably corresponds to a loss of adsorbed and bound water, proving the hydrophilic nature of CS. At 200 °C, the decomposition of the polymer starts, and it is indicated by the noticeable weight loss (about 60 %) between 200 °C and 400 °C that most likely results from the anhydro-glucosidic ring's dehydration (Hafizi, et al., 2023). In the thermograms of CSTPP@NPs, three stages of decomposition can be observed. The first occurred between 30 °C and 160 °C, which can be due to moisture loss, with a loss in weight of 6.4 %. This is followed by the second stage between 160 °C and 330 °C, which is probably attributed to the cleavage of glycosidic linkages via dehydration and deamination, corresponding to a weight loss of 19.1 %. At the end of the third stage (550 °C) a weight loss of 45% is registered, which is caused by the degradation of the polysaccharide backbone (Gomathi et al., 2017). In general, these findings confirm higher thermal stability

of CSTPP@NPs than that of pure CS, which can be attributed to interactions caused by the cross-linking of CS molecules with TPP. The TGA of Arg@NPs also depicts three phases for weight loss that are comparable to CSTPP@NPs. However, in the case of Arg@NPs, the remaining residue (50 %) was lower than the one of CSTPP@NPs (55 %). The additional weight losses at the second and third stages in the drug-loaded NPs can be assigned to the incorporation of Argireline in the CSTPP@NPs (Sabbagh et al., 2019).

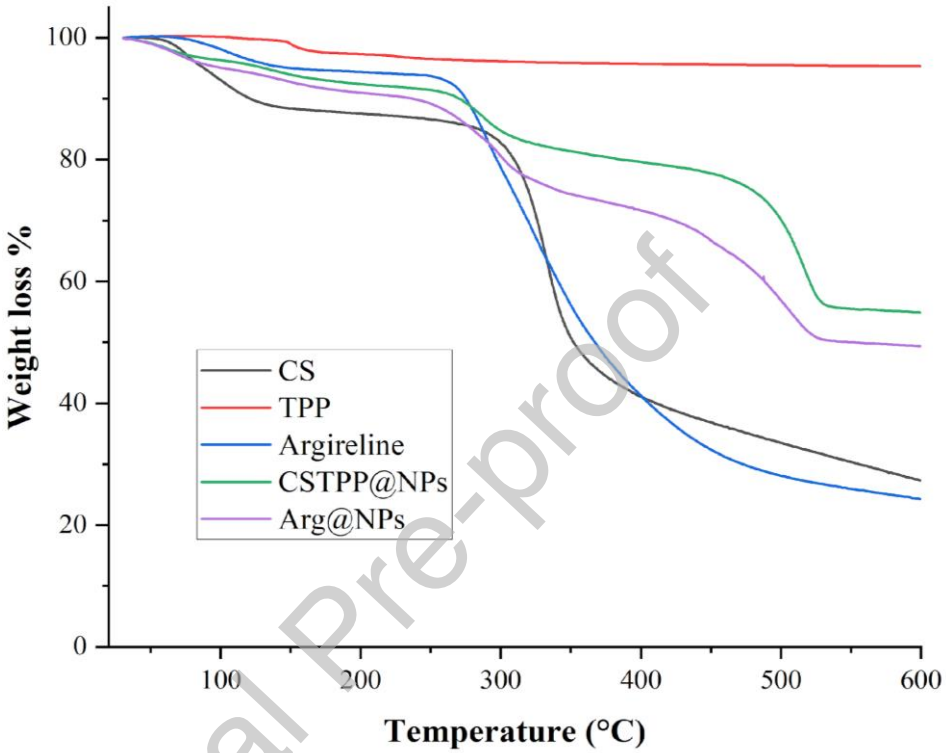

Figure 7. *Thermograms of CS, TPP, Argireline, CSTPP@NPs, and Arg@NPs.*

3.4 Physiochemical, rheological, and textural properties of Arg@NPs gel

Arg@NPs gel was successfully prepared to enhance the retention time of the nanoparticles at the skin surface facilitating the peptide delivery (Korkmaz et al., 2013). The produced gel appeared colorless and silky smooth to the touch, with a measured pH of 5.4 ± 0.2, which is considered acceptable for skin application (Lukić et al., 2021), and drug content of 99.2% ± 0.4.

To further understand its rheological properties the flow curve of the Arg@NPs gel was compared with that of the gel without nanoparticles (control sample) (Figure 8). To this end both flow curves were analyzed using power law (equation 5), Bingham (equation 6), Casson (equation 7), and Herschel–Bulkley (equation 8) models:

$\tau = k \cdot \dot{\gamma}^{n}$ (Eq. 5)

$\tau = \tau_0 + \eta \cdot \dot{\gamma}$ (Eq. 6)

$\tau^{0.5} = \tau_0^{0.5} + \eta^{0.5} \cdot \dot{\gamma}^{0.5}$

(Eq. 7) $\tau = \tau_0 + \kappa \cdot \dot{\gamma}^{\,n}$

(Eq. 8)

where τ is shear stress (Pa), $\dot{\gamma}$ is the shear rate (s^{-1}), τ_0 is yield stress (Pa), η is plastic viscosity (Pa·s), κ is consistency index ($Pa \cdot s^n$), and n is flow index.

The calculated R^2 for the control gel and Arg@NPs gel are listed in Table 4.

Table 4. *R^2 values resulting from the fitting of the flow curves of the control gel and Arg@NPs gel with different rheological models.*

Sample	**R^2**			
	Power law model	**Bingham model**	**Casson model**	**Herschel-Bulkley model**
Control gel	0.9979	0.9264	0.9585	0.9818
Arg@NPs gel	0.9990	0.8975	0.9524	0.9976

As can be seen in Table 4, based on the R^2 values, the best-fitting model for both flow curves is the power law model. The rheological parameters specific to this model were found an n value of 0.469 ± 0.003 and a k of 32.6 ± 0.4 ($Pa \cdot s^n$) for Arg@NPs gel, and an n value of 0.564 ± 0.006 and a k of 20.3 ± 0.5 ($Pa \cdot s^n$) for the control sample.

The flow index value smaller than 1 indicates a shear-thinning behavior (Ortan et al., 2011) that is considered an advantageous characteristic of topical semisolid systems since it allows the material to flow easily under relatively high shear rates facilitating the application (A-sasutjarit et al., 2005). Moreover, Arg@NPs contribute to significantly increasing the consistency index by strengthening the gel.

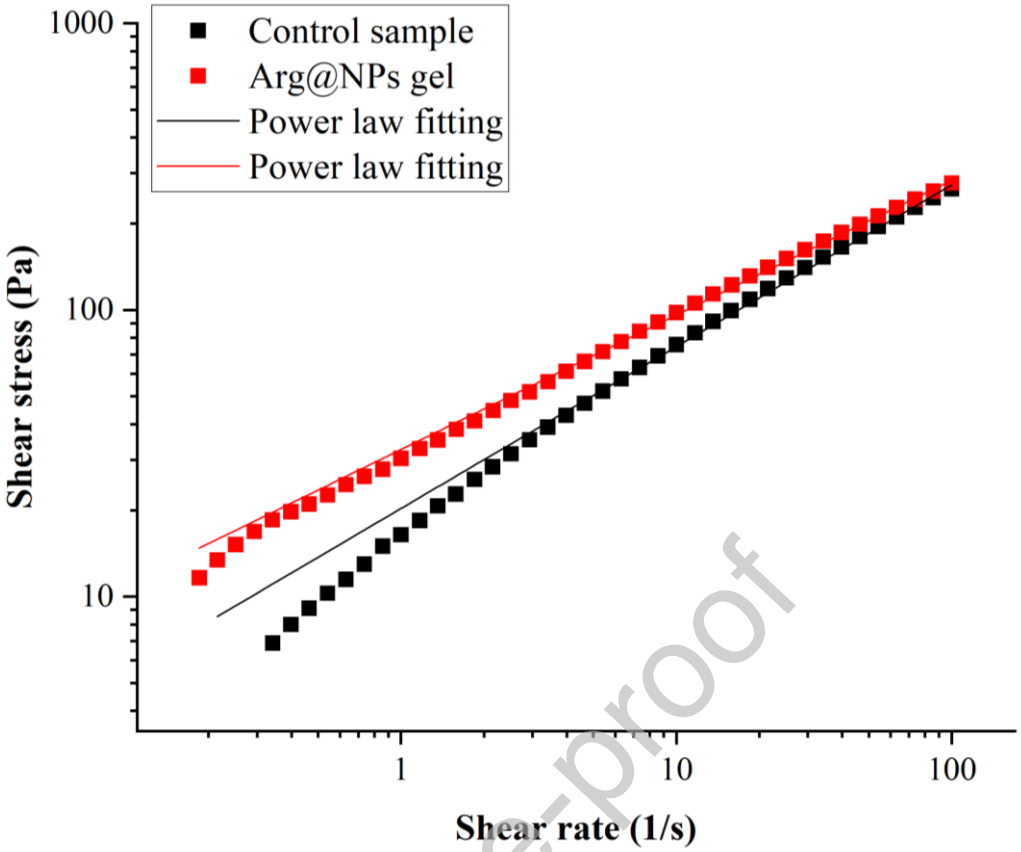

Figure 8. *Flow curves of Arg@NPs gel and control sample (gel without nanoparticles).*

Moreover, the texture profile of Arg@NPs gel was evaluated to determine mechanical parameters such as compressibility, hardness, adhesiveness, cohesiveness, and elasticity, which affect the performance of topical semisolid formulations. Figure 9 compares the force-time curves resulting from the texture profile analysis of Arg@NPs gel and gel without nanoparticles (control sample). The absence of shoulders in the curves' peaks indicates no point of rupture or obvious mechanical failure. In addition, a weakening of the internal structure is underlined by the fact that the second peak is smaller than the first (Rosenthal, 2010). The formulas used to calculate the mechanical properties of the gels are reported in the Box of Figure 9, while the calculated parameter values are listed in Table 5.

Briefly, hardness is defined as the force necessary to achieve a certain deformation, while compressibility represents the work required to deform the sample during the first compression of the probe. Arg@NPs gel showed low values of hardness and compressibility, indicating that it could be easily removed from the container and spread over the skin (Korkmaz et al., 2013). However, compared to the control sample, the gel loaded with the nanoparticles showed higher hardness and compressibility values and this agrees with the higher consistency index evaluated through rheological measurements. Hence, interactions between the gel and the nanoparticles contributed to strengthening the gel network (Ozcan et al., 2013).

Adhesiveness is defined as the work necessary to separate the probe from the sample and it is related to bioadhesion. Cohesiveness shows how repetitive shearing stresses affect the structural properties of the

formulations. Finally, the rate at which the deformed sample returns to its undeformed condition is represented by the elasticity value. Compared to the control sample, Arg@NPs gel showed a slightly higher adhesiveness and, thus, appropriate retention at the application site, leading to higher absorptivity (Rai et al., 2014). The cohesiveness values for both Arg@NPs gel and control sample were close to unity, indicating that the gel matrix was not broken during the first compression and, consequently, the same energy was required by the probe to enter the gel matrix during the second compression (Carvalho et al., 2012). Finally, both formulations exhibited an acceptable elasticity value compared with previous literature findings (Ay Şenyiğit et al., 2015, Ozcan et al., 2013, Cevher et al., 2008).

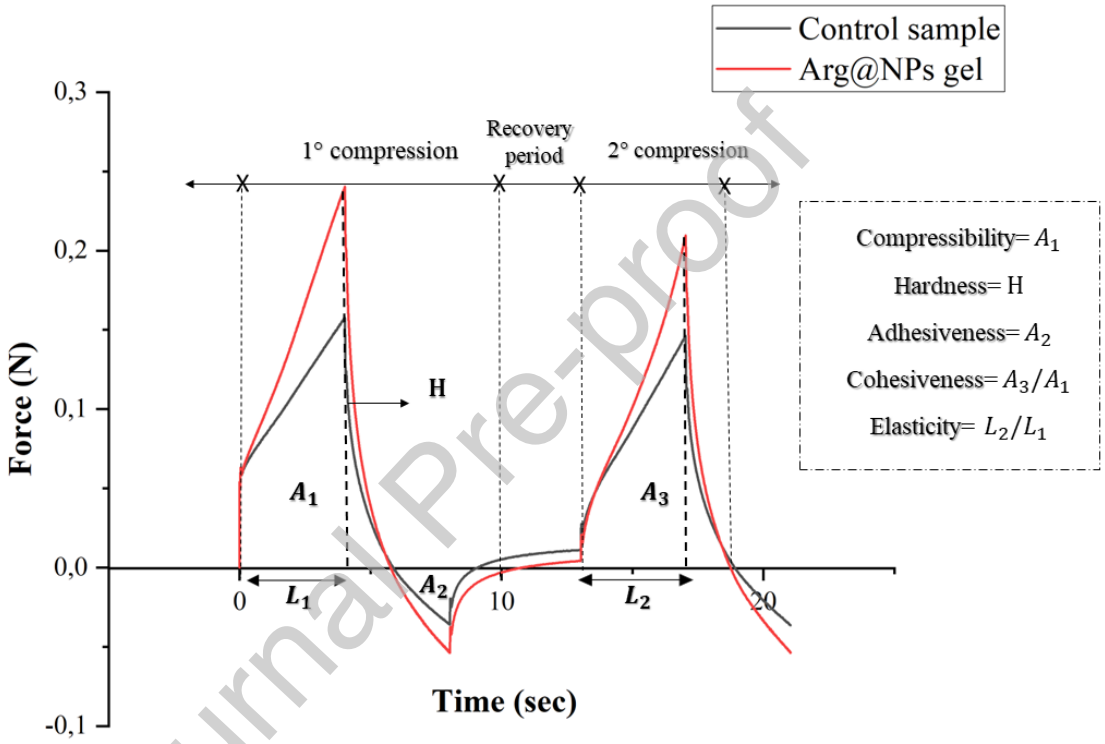

Figure 9. *Texture profile analysis graph of Arg@NPs gel and control sample (gel without nanoparticles).*

Table 5. *Mechanical properties of Arg@NPs gel and control sample (gel without nanoparticles).*

	Compressibility (N·mm)	Hardness (N)	Adhesiveness (N·mm)	Cohesiveness	Elasticity
Control sample	0.34 ± 0.02	0.14 ± 0.01	0.05 ± 0.01	1.25 ± 0.01	1.02 ± 0.02
Arg@NPs gel	0.52 ± 0.04	0.22 ± 0.01	0.09 ± 0.01	0.98 ± 0.03	1.02 ± 0.01

3.5 Argireline release from Arg@NPs and Arg@NPs gel

Drug release studies were carried out in PBS (pH 7.4) at 32 °C to mimic the physiological conditions. Figure 10 illustrates the cumulative percentage of Argireline released from Arg@NPs and Arg@NPs gel over 48 hours. Both formulations exhibited a biphasic pattern characterized by an initial fast release followed by a period of much slower and sustained release. The ‘’burst’’ phase occurred in the first 2 hours and was presumably caused by a rapid release of Argireline trapped or adsorbed on the outer layer of NPs. The subsequent slowing of the release rate was instead due to the diffusion of drug molecules through the CS matrix (He et al., 2020, Wu et al., 2017). In the Arg@NPs gel, drug release from the NPs occurred first and then diffused through the gel matrix, producing a further sustained release effect (Ullah et al., 2022). Indeed, at the end of the 48 hours of incubation, 40.3 % ± 0.9 and 32.2 % ± 0.3 of Argireline was released from Arg@NPs and Arg@NPs gel respectively. Furthermore, this overall low drug release from both formulations can be explained by the influence of the pH of the release medium on the release rate from CSTPP@NPs. In fact, previous findings (Papadimitriou et al., 2008, Makhlof et al., 2011, Zhang et al., 2004) revealed that in an acidic environment, the ionic interaction between CS and TPP weakens and CS dissolves quickly, allowing for faster drug release from NPs in a low pH medium than at pH 7.4.

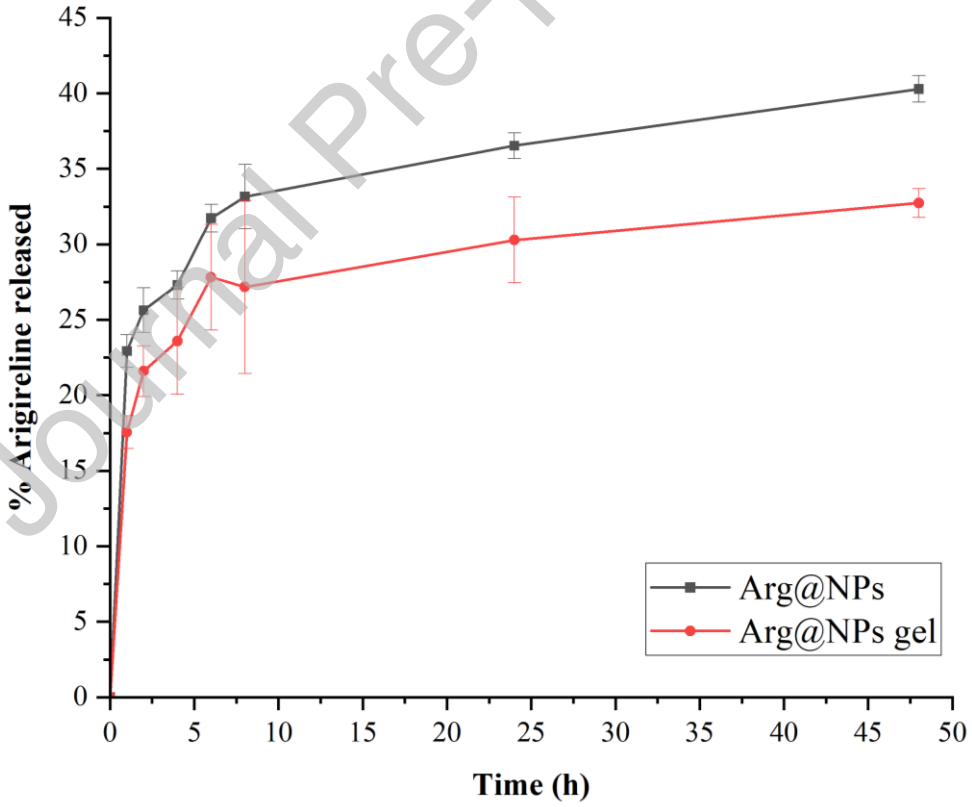

***Figure 10**. Argireline cumulative release from Arg@NPs and Arg@NPs gel. Data are presented as mean ± SD, where n = 3.*

3.6 Kinetic of drug release from Arg@NPs and Arg@NPs gel

To understand the kinetics of Argireline release from Arg@NPs and Arg@NPs gel, drug release data were fitted by the first-order, Higuchi, Korsmeyer-Peppas, and Peppas-Salhin models. The simulated equations, their respective kinetic constants, and the correlation coefficients (R^2) are listed in Table 6, where k_1 is the first-order rate constant, K_H is the dissolution constant, k is the release-rate constant, K_d is the Fickian diffusional contribution, and K_r is the matrix swelling contribution (Khorshid et al., 2022).

Table 6. Kinetic parameters resulting from fitting experimental Argireline release data with different kinetic equations.

Sample	Mathematical model	Kinetic constants	R^2
Arg@NPs	First-order: $\frac{M_t}{M_0} = e^{-k_1 t}$	$k_1 = 0.62 \pm 0.17$	0.79
	Higuchi: $\frac{M_t}{M_0} = K_H\sqrt{t}$	$K_H = 17.91 \pm 0.93$	0.88
	Korsmeyer-Peppas: $\frac{M_t}{M_0} = kt^n$	$k = 23.49 \pm 0.64$ $n = 0.14 \pm 0.01$	0.99
	Peppas-Salhin: $\frac{M_t}{M_0} = K_d t^m + k_r t^{2m}$	$K_d = 26.97 \pm 0.97$ K_r = -4.28 ± 0.62	0.99
Arg@NPs gel	First-order: $\frac{M_t}{M_0} = e^{-k_1 t}$	$k_1 = 0.58 \pm 0.18$	0.81
	Higuchi: $\frac{M_t}{M_0} = K_H\sqrt{t}$	$K_H = 14.86 \pm 0.84$	0.86
	Korsmeyer-Peppas: $\frac{M_t}{M_0} = kt^n$	$k = 19.63 \pm 0.88$ $n = 0.13 \pm 0.02$	0.98
	Peppas-Salhin: $\frac{M_t}{M_0} = K_d t^m + K_r t^{2m}$	$K_d = 21.97 \pm 1.19$ K_r = -3.74 ± 0.42	0.99

As can be seen in Table 6 and Figure 11, the drug release profile of Arg@NPs and Arg@NPs gel best fitted the Korsmeyer-Peppas and Peppas-Salhin models as indicated by the R^2 values. In the Korsmeyer-Peppas model, the value of the release exponent (n) was below 0.5, indicating a Fickian diffusion mechanism of Argireline release from both formulations. This is also confirmed by the Peppas-Salhin model, in which the not-significant negative value of K_r means that any significant contribution of the matrix swelling or erosion occurs (Maurizii et al., 2023).

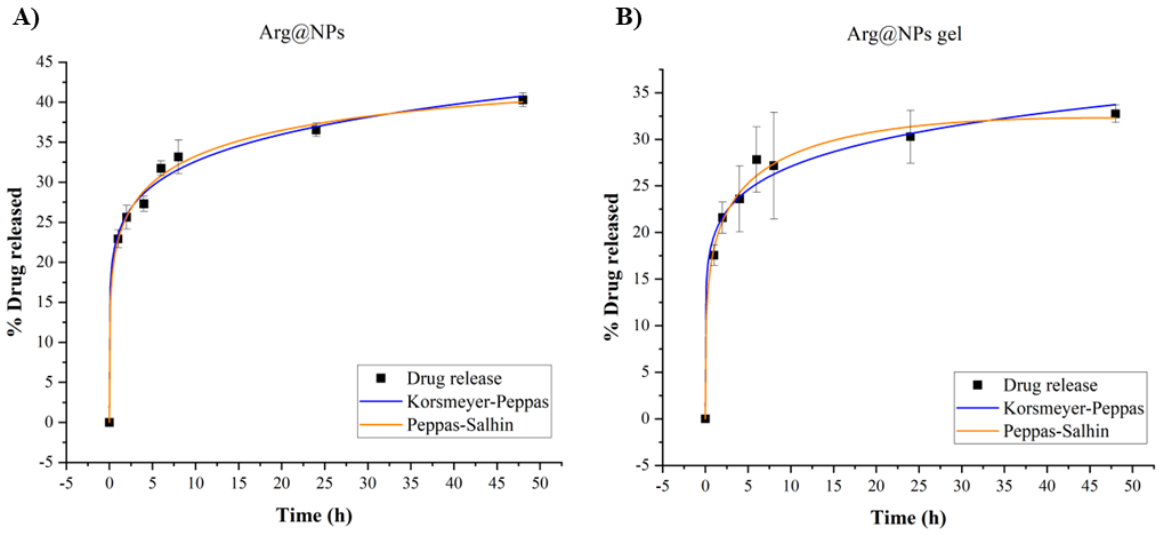

Figure 11. *Release data of Argireline from A) Arg@NPs and B) Arg@NPs gel fitting to Korsmeyer-Peppas and Peppas-Salhin models.*

3.7 In vitro permeation studies through Strat-M® membranes

The in vitro Arg@NPs and Arg@NPs gel permeation behavior was determined using Franz-type diffusion cells. Free Argireline solution was used as the control. Strat-M® were mounted as partitioning membranes since they were extensively reported to mimic the morphology and the lipid chemistry of human skin (Haq et al., 2018). According to the in vitro drug release studies' results, both Arg@NPs and Arg@NPs gel showed a biphasic permeation pattern (Figure 12), indicating the initial rapid partitioning of Argireline close to the NPs surface which was followed by gradual diffusion of the drug trapped into the CS matrix (Hasanovic et al., 2009). As shown in Figure 12, Argireline reached a higher membrane permeation when encapsulated in CS NPs. After 48 hours of experimentation, the cumulative amount of Arigireline permeated was 110.66 ± 9.27 µg/cm^2 for free Argireline solution and 472.70 ± 27.63 µg/cm^2 for Arg@NPs. Indeed, it was already reported that chitosan forms hydrogen bonding with the lipids blend of the top layer of the Strat-M® membrane, facilitating the deposition of the nanoparticles in the membrane's surface and thus enhancing the peptide permeation (Campos et al., 2022). Moreover, considering the low average particle size of the produced Arg@NPs, they could enhance the penetration of the encapsulated peptide through the skin thanks to the ability of small polymeric nanoparticles (particle size < 200 nm) to deposit in the hair follicles, producing a high local concentration of the encapsulated drug which can then diffuse into the surrounding skin cells (Desai et al., 2010). Finally, after 48 hours of experimentation, the cumulative amount of Argireline permeated was lower for Arg@NPs gel (330.66 ± 37.23 µg/cm^2) than for Arg@NPs, since the additional diffusion of the peptide through the gel matrix has delayed its permeation through the membrane. Overall, having Arg@NPs gel a better control over peptide release, it could provide the skin with the peptide over a longer period than Arg@NPs (Al-Kassas et al., 2016).

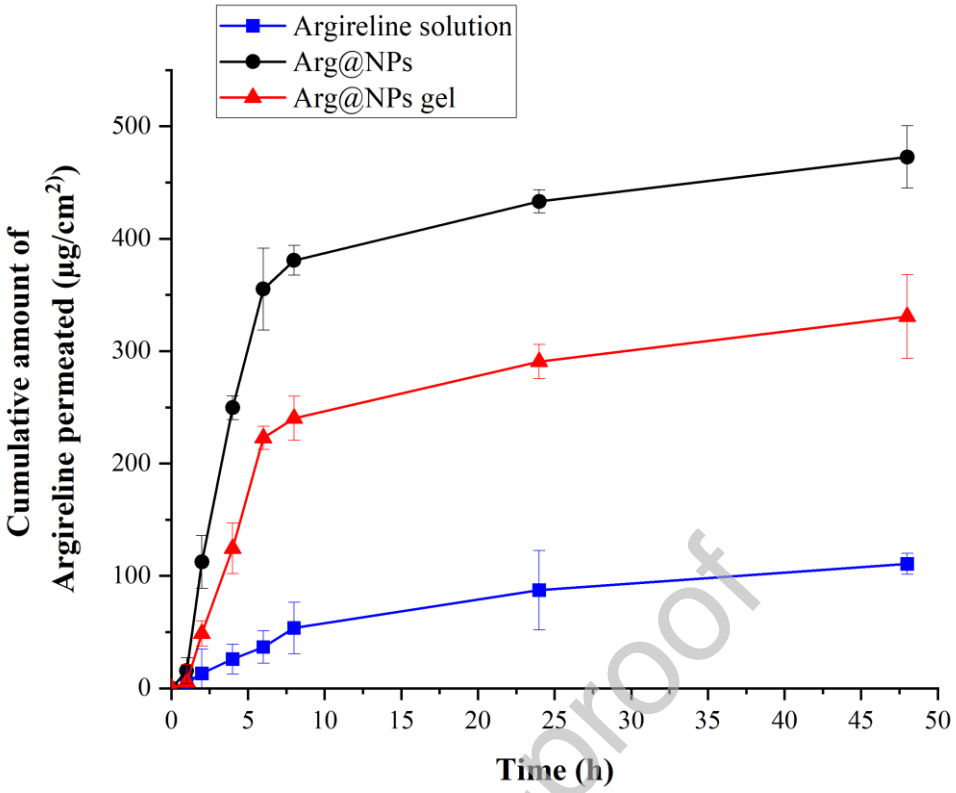

Figure 12. *In vitro* permeation profiles of Argireline solution, Arg@NPs suspension, and Arg@NPs gel through Strat-M® membrane.

3.8 Stability of Arg@NPs and Arg@NPs gel

The stability of Arg@NPs and Arg@NPs gel was tested by keeping the formulations at room and refrigerator temperature for one month and evaluating them periodically (0, 15, and 30 days). NPs formulation was evaluated for size, PDI, and EE %, while gel formulation for pH, drug content, and rheological and mechanical properties. During storage time, a higher increase in NPs size was observed for formulation kept at room temperature compared to that stored in the refrigerator (Table 7), which may be due to the spontaneous aggregation of nanoparticles. In fact, a temperature of about 4 °C was reported to reduce the aggregation rate compared to room temperature, most likely by lowering the frequency of particle collisions (López-León et al., 2005; Morris et al., 2011). Moreover, the EE % decreased negligibly after one month (Table 7), indicating that the formulation was chemically stable at both storage conditions (Vaghasiya et al., 2013). Similarly, little variation in pH and drug content of Arg@NPs gel was observed (Table 8), demonstrating its stability. Finally, no significant differences were found in the rheological and mechanical parameters calculated during the storage of the gel both at room and refrigerator temperature ($p > 0.05$) (data not shown).

Table 7. *Stability data of Arg@NPs showing the change in % encapsulation efficiency (EE%) and particle size (nm) when stored at different temperature conditions.*

	EE%		**Particle size (nm)**	
	Room temp. (25 ± 2 °C)	**Refrigerator temp. (2-4 °C)**	**Room temp. (25 ± 2 °C)**	**Refrigerator temp. (2-4 °C)**
Initial	90.2 ± 0.7	90.2 ± 0.7	186.0 ± 1.2	186.0 ± 1.2
After 15 days	89.1 ± 0.1	89.8 ± 0.2	194.2 ± 2.7	189.3 ± 4.1
After 30 days	88.2 ± 0.5	89.5 ± 0.1	203.8 ± 6.3	192.7 ± 1.9

Table 8. *Stability data of Arg@NPs gel showing the change in % drug content and pH when stored at different temperature conditions.*

	% Drug content		**pH**	
	Room temp. (25 ± 2 °C)	**Refrigerator temp. (2-4 °C)**	**Room temp. (25 ± 2 °C)**	**Refrigerator temp. (2-4 °C)**
Initial	99.2 ± 0.4	99.2 ± 0.4	5.4 ± 0.2	5.4 ± 0.2
After 15 days	97.9 ± 0.5	98.9 ± 0.2	5.3 ± 0.1	5.5 ± 0.1
After 30 days	96.5 ± 1.2	98.2 ± 0.2	5.3 ± 0.2	5.4 ± 0.1

4. Conclusions

This study demonstrated that the microfluidic-assisted ionotropic gelation method is a robust and reproducible platform for the manufacturing of peptide-loaded CS-TPP NPs. By using a custom-designed microfluidic chip and by tuning process parameters (pH, TFR, and CS and TPP concentration), nanoparticles with small size, narrow size distribution, and long-term stability have been prepared. Argireline, a model peptide, was successfully encapsulated (90 % of EE %) in the optimized CSTPP NPs, and the results confirmed nanoformulation's ability to regulate the release of the peptide. Moreover, considering a potential topical application of the Argireline-loaded CS-TPP NPs, the formulation was gelled to increase its retention time at the skin surface, facilitating peptide delivery. The formulated gel showed suitable mechanical characteristics (e.g. hardness, compressibility, adhesiveness, cohesiveness, and elasticity) for transdermal administration of Argireline and better control over its release and permeation through the skin. Hence,

Argireline-loaded CSTPP NPs assembled via microfluidic mixing could represent a promising strategy for non-invasive peptide delivery.

Credit authorship

Conflict of interest

The authors declare no conflict of interest.

Funding

This work has been funded by the European Union – NextGenerationEU under the Italian Ministry of University and Research (MUR) National Innovation Ecosystem grant ECS00000041 - VITALITY - CUP H33C22000430006

Sofia Moroni acknowledges Marche Region for the PhD scholarship (Innovative doctoral program POR Marche FSE 2014/2020 D.R. 354/2020)

Acknowledgments

We acknowledge ITIS E. Mattei (Urbino, PU, Italy) for the utilization of the FT-IR instrument.

References

A-sasutjarit, R., Sirivat, A., & Vayumhasuwan, P. (2005). Viscoelastic properties of Carbopol 940 gels and their relationships to piroxicam diffusion coefficients in gel bases. Pharmaceutical Research, 22(12), 2134–2140. https://doi.org/10.1007/s11095-005-8244-2

Agrahari, V., Agrahari, V., & Mitra, A. K. (2016). Nanocarrier Fabrication and macromolecule drug delivery: Challenges and opportunities. Therapeutic Delivery, 7(4), 257–278. https://doi.org/10.4155/tde-2015-0012

Al-Kassas, R., Wen, J., Cheng, A. E.-M., Kim, A. M.-J., Liu, S. S., & Yu, J. (2016). Transdermal delivery of propranolol hydrochloride through chitosan nanoparticles dispersed in Mucoadhesive Gel. Carbohydrate Polymers, 153, 176–186. https://doi.org/10.1016/j.carbpol.2016.06.096

Ay Şenyiğit, Z., Karavana, S. Y., Ilem Ozdemir, D., Caliskan, C., Waldner, C., Sen, S., Bernkop-Schnürch, A., & Baloglu, E. (2015). Design and evaluation of an intravesical delivery system for superficial bladder cancer: preparation of gemcitabine HCl-loaded chitosan–thioglycolic acid nanoparticles and comparison of chitosan/poloxamer gels as carriers. International Journal of Nanomedicine, 6493. https://doi.org/10.2147/ijn.s93750

Bajracharya, R., Song, J. G., Back, S. Y., & Han, H.-K. (2019). Recent advancements in non-invasive formulations for protein drug delivery. Computational and Structural Biotechnology Journal, 17, 1290–1308. https://doi.org/10.1016/j.csbj.2019.09.004

Carvalho, F. C., Calixto, G., Hatakeyama, I. N., Luz, G. M., Gremião, M. P., & Chorilli, M. (2012). Rheological, mechanical, and bioadhesive behavior of hydrogels to optimize skin delivery systems. Drug Development and Industrial Pharmacy, 39(11), 1750–1757. https://doi.org/10.3109/03639045.2012.734510

Campana, R., Casettari, L., Ciandrini, E., Illum, L., & Baffone, W. (2017). Chitosans inhibit the growth and the adhesion of Klebsiella pneumoniae and Escherichia coli clinical isolates on urinary catheters. International Journal of Antimicrobial Agents, 50(2), 135–141. https://doi.org/10.1016/j.ijantimicag.2017.03.031

Campos, E. V., Proença, P. L., da Costa, T. G., de Lima, R., Fraceto, L. F., & de Araujo, D. R. (2022). Using chitosan-coated polymeric nanoparticles-thermosensitive hydrogels in association with limonene as Skin Drug Delivery Strategy. BioMed Research International, 2022, 1–18. https://doi.org/10.1155/2022/9165443

Casettari, L., Gennari, L., Angelino, D., Ninfali, P., & Castagnino, E. (2012). ORAC of chitosan and its derivatives. Food Hydrocolloids, 28(2), 243–247. https://doi.org/10.1016/j.foodhyd.2012.01.005

Cevher, E., Taha, M. A. M., Orlu, M., & Araman, A. (2008). Evaluation of mechanical and mucoadhesive properties of clomiphene citrate gel formulations containing carbomers and their thiolated derivatives. Drug Delivery, 15(1), 57–67. https://doi.org/10.1080/10717540701829234

Chiesa, E., Riva, F., Dorati, R., Greco, A., Ricci, S., Pisani, S., Patrini, M., Modena, T., Conti, B., & Genta, I. (2020). On-Chip Synthesis of Hyaluronic Acid-Based Nanoparticles for Selective Inhibition of CD44+ Human Mesenchymal Stem Cell Proliferation. Pharmaceutics, 12(3), 260. https://doi.org/10.3390/pharmaceutics12030260

Chiesa, E., Greco, A., Riva, F., Dorati, R., Conti, B., Modena, T., & Genta, I. (2021). Hyaluronic Acid-Based Nanoparticles for Protein Delivery: Systematic Examination of Microfluidic Production Conditions. Pharmaceutics, 13(10), 1565. https://doi.org/10.3390/pharmaceutics13101565

de Carvalho, F. G., Magalhães, T. C., Teixeira, N. M., Gondim, B. L., Carlo, H. L., dos Santos, R. L., de Oliveira, A. R., & Denadai, Â. M. (2019). Synthesis and characterization of TPP/chitosan nanoparticles: Colloidal mechanism of reaction and antifungal effect on C. albicans biofilm formation. Materials Science and Engineering: C, 104, 109885. https://doi.org/10.1016/j.msec.2019.109885

Desai, P., Patlolla, R. R., & Singh, M. (2010). Interaction of nanoparticles and cell-penetrating peptides with skin for transdermal drug delivery. Molecular Membrane Biology, 27(7), 247–259. https://doi.org/10.3109/09687688.2010.522203

Du, Z., Liu, J., Zhang, T., Yu, Y., Zhang, Y., Zhai, J., Huang, H., Wei, S., Ding, L., & Liu, B. (2019). A study on the preparation of chitosan-tripolyphosphate nanoparticles and its entrapment mechanism for egg white derived peptides. Food Chemistry, 286, 530–536. https://doi.org/10.1016/j.foodchem.2019.02.012

Fan, W., Yan, W., Xu, Z., & Ni, H. (2012). Formation mechanism of monodisperse, low molecular weight chitosan nanoparticles by Ionic gelation technique. Colloids and Surfaces B: Biointerfaces, 90, 21–27. https://doi.org/10.1016/j.colsurfb.2011.09.042

Farahani, M., Moradikhah, F., Shabani, I., Soflou, R. K., & Seyedjafari, E. (2021). Microfluidic fabrication of berberine-loaded nanoparticles for cancer treatment applications. Journal of Drug Delivery Science and Technology, 61, 102134. https://doi.org/10.1016/j.jddst.2020.102134

Gadziński, P., Froelich, A., Jadach, B., Wojtyłko, M., Tatarek, A., Białek, A., Krysztofiak, J., Gackowski, M., Otto, F., & Osmałek, T. (2022). Ionotropic gelation and chemical crosslinking as methods for fabrication of modified-release Gellan Gum-based drug delivery systems. Pharmaceutics, 15(1), 108. https://doi.org/10.3390/pharmaceutics15010108

Gomathi, T., Sudha, P. N., Florence, J. A., Venkatesan, J., & Anil, S. (2017). Fabrication of letrozole formulation using chitosan nanoparticles through Ionic gelation method. International Journal of Biological Macromolecules, 104, 1820–1832. https://doi.org/10.1016/j.ijbiomac.2017.01.147

Greco, A., Gabold, B., Chen, S., Wang, X., Xu, Z., Hartschuh, A., Chiesa, E., Genta, I., Ried, C., Merdan, T., & Merkel, O. (2023). Microfluidic Mixing as Platform Technology for Production of Chitosan Nanoparticles Loaded with Different Macromolecules. https://doi.org/10.2139/ssrn.4381305

Hafizi, T., Shahriari, M. H., Abdouss, M., & Kahdestani, S. A. (2023). Synthesis and Characterization of Vancomycin-Loaded Chitosan Nanoparticles for Drug Delivery. Polymer Bulletin, 80, 5607-5621. https://doi.org/10.1007/s00289-022-04237-8

Haq, A., Goodyear, B., Ameen, D., Joshi, V., & Michniak-Kohn, B. (2018). Strat-M® synthetic membrane: Permeability comparison to human cadaver skin. International Journal of Pharmaceutics, 547(1–2), 432–437. https://doi.org/10.1016/j.ijpharm.2018.06.012

Hasanovic, A., Zehl, M., Reznicek, G., & Valenta, C. (2009). Chitosan-tripolyphosphate nanoparticles as a possible skin drug delivery system for aciclovir with enhanced stability. Journal of Pharmacy and Pharmacology, 61(12), 1609–1616. https://doi.org/10.1211/jpp.61.12.0004

Hashad, R. A., Ishak, R. A. H., Fahmy, S., Mansour, S., & Geneidi, A. S. (2016). Chitosan-tripolyphosphate nanoparticles: Optimization of formulation parameters for improving process yield at a novel ph using artificial neural networks. International Journal of Biological Macromolecules, 86, 50–58. https://doi.org/10.1016/j.ijbiomac.2016.01.042

He, T., Wang, W., Chen, B., Wang, J., Liang, Q., & Chen, B. (2020). 5-fluorouracil monodispersed chitosan microspheres: Microfluidic chip fabrication with crosslinking, characterization, drug release and anticancer activity. Carbohydrate Polymers, 236, 116094. https://doi.org/10.1016/j.carbpol.2020.116094

Hickey, J. W., Santos, J. L., Williford, J.-M., & Mao, H.-Q. (2015). Control of polymeric nanoparticle size to improve therapeutic delivery. Journal of Controlled Release, 219, 536–547. https://doi.org/10.1016/j.jconrel.2015.10.006

Hosseini, S. F., Soleimani, M. R., & Nikkhah, M. (2018). Chitosan/sodium tripolyphosphate nanoparticles as efficient vehicles for antioxidant peptidic fraction from common Kilka. International Journal of Biological Macromolecules, 111, 730–737. https://doi.org/10.1016/j.ijbiomac.2018.01.023

Jonassen, H., Kjøniksen, A.-L., & Hiorth, M. (2012). Effects of ionic strength on the size and compactness of chitosan nanoparticles. Colloid and Polymer Science, 290(10), 919–929. https://doi.org/10.1007/s00396-012-2604-3

Khoerunnisa, F., Nurhayati, M., Dara, F., Rizki, R., Nasir, M., Aziz, H. A., Hendrawan, H., Poh, N. E., Kaewsaneha, C., & Opaprakasit, P. (2021). Physicochemical properties of TPP-crosslinked chitosan nanoparticles as potential antibacterial agents. Fibers and Polymers, 22(11), 2954–2964. https://doi.org/10.1007/s12221-021-0397-z

Khorshid, S., Montanari, M., Benedetti, S., Moroni, S., Aluigi, A., Canonico, B., Papa, S., Tiboni, M., & Casettari, L. (2022). A microfluidic approach to fabricate sucrose decorated liposomes with increased uptake in breast cancer cells. European Journal of Pharmaceutics and Biopharmaceutics, 178, 53–64. https://doi.org/10.1016/j.ejpb.2022.07.015

Korkmaz, E., Gokce, E. H., & Ozer, O. (2013). Development and evaluation of coenzyme Q10 loaded solid lipid nanoparticle hydrogel for Enhanced Dermal Delivery. Acta Pharmaceutica, 63(4), 517–529. https://doi.org/10.2478/acph-2013-0039

Kumari, A., Yadav, S. K., & Yadav, S. C. (2010). Biodegradable polymeric nanoparticles based drug delivery systems. Colloids and Surfaces B: Biointerfaces, 75 (1), 1-18. https://doi.org/10.1016/j.colsurfb.2009.09.001

López-León, T., Carvalho, E. L. S., Seijo, B., Ortega-Vinuesa, J. L., & Bastos-González, D. (2005). Physicochemical characterization of chitosan nanoparticles: Electrokinetic and stability behavior. Journal of Colloid and Interface Science, 283(2), 344–351. https://doi.org/10.1016/j.jcis.2004.08.186

Loutfy, S. A., Alam El-Din, H. M., Elberry, M. H., Allam, N. G., Hasanin, M. T., & Abdellah, A. M. (2016). Synthesis, characterization and cytotoxic evaluation of chitosan nanoparticles: in vitro liver cancer model. Advances in Natural Sciences: Nanoscience and Nanotechnology, 7(3), 035008. https://doi.org/10.1088/2043-6262/7/3/035008

Lukić, M., Pantelić, I., & Savić, S. D. (2021). Towards optimal pH of the skin and topical formulations: From the current state of the art to tailored products. Cosmetics, 8(3), 69. https://doi.org/10.3390/cosmetics8030069

Lustriane, C., Dwivany, F. M., Suendo, V., & Reza, M. (2018). Effect of chitosan and chitosan-nanoparticles on post harvest quality of banana fruits. Journal of Plant Biotechnology, 45(1), 36–44. https://doi.org/10.5010/jpb.2018.45.1.036

Makhlof, A., Tozuka, Y., & Takeuchi, H. (2011). Design and evaluation of novel ph-sensitive chitosan nanoparticles for oral insulin delivery. European Journal of Pharmaceutical Sciences, 42(5), 445–451. https://doi.org/10.1016/j.ejps.2010.12.007

Maruyama, C. R., Guilger, M., Pascoli, M., Bileshy-José, N., Abhilash, P. C., Fraceto, L. F., & De Lima, R. (2016). Nanoparticles based on chitosan as carriers for the combined herbicides Imazapic and Imazapyr. Scientific Reports, 6(1). https://doi.org/10.1038/srep19768

Masarudin, M. J., Cutts, S. M., Evison, B. J., Phillips, Don. R., & Pigram, P. J. (2015). Factors determining the stability, size distribution, and cellular accumulation of small, monodisperse chitosan nanoparticles as candidate vectors for anticancer drug delivery: Application to the passive encapsulation of [^{14}C]-doxorubicin. Nanotechnology, Science and Applications, 67. https://doi.org/10.2147/nsa.s91785

Maurizii, G., Moroni, S., Khorshid, S., Aluigi, A., Tiboni, M., & Casettari, L. (2023). 3D-printed EVA-based patches manufactured by direct powder extrusion for personalized transdermal therapies. International Journal of Pharmaceutics, 635, 122720. https://doi.org/10.1016/j.ijpharm.2023.122720

Mikušová, V., & Mikuš, P. (2021). Advances in chitosan-based nanoparticles for Drug Delivery. International Journal of Molecular Sciences, 22(17), 9652. https://doi.org/10.3390/ijms22179652

Morris, G. A., Castile, J., Smith, A., Adams, G. G., & Harding, S. E. (2011). The effect of prolonged storage at different temperatures on the particle size distribution of Tripolyphosphate (TPP) – Chitosan nanoparticles. Carbohydrate Polymers, 84(4), 1430–1434. https://doi.org/10.1016/j.carbpol.2011.01.044

Ortan, A., Parvu, C. D., Ghica, M. V., Popescu, L. M., & Ionita, L. (2011). Rheological Study of a Liposomal Hydrogel Based On Carbopol. Romanian Biotechnological Letters, 16(1).

Ozcan, I., Azizoglu, E., Senyigit, T., Ozyazici, & Ozer, O. (2013). Enhanced dermal delivery of diflucortolone valerate using lecithin/chitosan nanoparticles: In-vitro and in-vivo evaluations. International Journal of Nanomedicine, 461. https://doi.org/10.2147/ijn.s40519

Pagels, R. F., & Prud'homme, R. K. (2015). Polymeric nanoparticles and microparticles for the delivery of peptides, biologics, and soluble therapeutics. Journal of Controlled Release, 219, 519–535. https://doi.org/10.1016/j.jconrel.2015.09.001

Papadimitriou, S., Bikiaris, D., Avgoustakis, K., Karavas, E., & Georgarakis, M. (2008). Chitosan nanoparticles loaded with dorzolamide and pramipexole. Carbohydrate Polymers, 73(1), 44–54. https://doi.org/10.1016/j.carbpol.2007.11.007

Patel, A., Patel, M., Yang, X., & Mitra, A. (2014). Recent advances in protein and peptide drug delivery: A special emphasis on polymeric nanoparticles. Protein & Peptide Letters, 21(11), 1102–1120. https://doi.org/10.2174/0929866521666140807114240

Rai, V. K., Yadav, N. P., Sinha, P., Mishra, N., Luqman, S., Dwivedi, H., Kymonil, K. M., & Saraf, S. A. (2014). Development of cellulosic polymer based gel of novel ternary mixture of miconazole nitrate for buccal delivery. Carbohydrate Polymers, 103, 126–133. https://doi.org/10.1016/j.carbpol.2013.12.019

Rampino, A., Borgogna, M., Blasi, P., Bellich, B., & Cesàro, A. (2013). Chitosan nanoparticles: Preparation, size evolution and stability. International Journal of Pharmaceutics, 455(1–2), 219–228. https://doi.org/10.1016/j.ijpharm.2013.07.034

Rázga, F., Vnuková, D., Némethová, V., Mazancová, P., & Lacík, I. (2016). Preparation of chitosan-TPP sub-micron particles: Critical evaluation and derived recommendations. Carbohydrate Polymers, 151, 488–499. https://doi.org/10.1016/j.carbpol.2016.05.092

Rosenthal, A. J. (2010). Texture profile analysis - how important are the parameters? Journal of Texture Studies, 41(5), 672–684. https://doi.org/10.1111/j.1745-4603.2010.00248.x

Sabbagh, H. A., Abudayeh, Z., Abudoleh, S. M., Alkrad, J. A., Hussein, M. Z., & Hussein-Al-Ali, S. H. (2019). Application of multiple regression analysis in optimization of metronidazole-chitosan nanoparticles. Journal of Polymer Research, 26(8), 205. https://doi.org/10.1007/s10965-019-1854-x

Singh, V., & Chaubey, N. (2019). Design and evaluation of topical hydrogel formulation of aceclofenac for improved therapy. Journal of Drug Delivery and Therapeutics, 9(5), 118–122. https://doi.org/10.22270/jddt.v9i5.3605

Soheili, S., Mandegar, E., Moradikhah, F., Doosti-Telgerd, M., & Javar, H. A. (2021). Experimental and numerical studies on microfluidic preparation and engineering of chitosan nanoparticles. Journal of Drug Delivery Science and Technology, 61, 102268. https://doi.org/10.1016/j.jddst.2020.102268

Sommonte, F., Arduino, I., Iacobazzi, R. M., Tiboni, M., Catalano, F., Marotta, R., Di Francesco, M., Casettari, L., Decuzzi, P., Lopedota, A. A., & Denora, N. (2023). Microfluidic assembly of "Turtle-Like" shaped solid lipid nanoparticles for lysozyme delivery. International Journal of Pharmaceutics, 631, 122479. https://doi.org/10.1016/j.ijpharm.2022.122479

Tai, A., Bianchini, R., & Jachowicz, J. (2014). Texture analysis of Cosmetic/pharmaceutical raw materials and formulations. International Journal of Cosmetic Science, 36(4), 291–304. https://doi.org/10.1111/ics.12125

Tiboni, M., Tiboni, M., Pierro, A., Del Papa, M., Sparaventi, S., Cespi, M., & Casettari, L. (2021). Microfluidics for Nanomedicines Manufacturing: An affordable and low-cost 3D printing approach. International Journal of Pharmaceutics, 599, 120464. https://doi.org/10.1016/j.ijpharm.2021.120464

Ullah, K. H., Rasheed, F., Naz, I., Ul Haq, N., Fatima, H., Kanwal, N., & Ur-Rehman, T. (2022). Chitosan nanoparticles loaded poloxamer 407 gel for transungual delivery of Terbinafine HCL. Pharmaceutics, 14(11), 2353. https://doi.org/10.3390/pharmaceutics14112353

Vaghasiya, H., Kumar, A., & Sawant, K. (2013). Development of solid lipid nanoparticles based controlled release system for topical delivery of terbinafine hydrochloride. European Journal of Pharmaceutical Sciences, 49(2), 311–322. https://doi.org/10.1016/j.ejps.2013.03.013

Wu, J., Wang, Y., Yang, H., Liu, X., & Lu, Z. (2017). Preparation and biological activity studies of resveratrol loaded ionically cross-linked Chitosan-TPP nanoparticles. Carbohydrate Polymers, 175, 170–177. https://doi.org/10.1016/j.carbpol.2017.07.058

Yan, Q., Weng, J., Wu, X., Wang, W., Yang, Q., Guo, F., Wu, D., Song, Y., Chen, F., & Yang, G. (2020). Characteristics, cryoprotection evaluation and in vitro release of BSA-loaded chitosan nanoparticles. Marine Drugs, 18(6), 315. https://doi.org/10.3390/md18060315

Zielińska, A., Carreiró, F., Oliveira, A. M., Neves, A., Pires, B., Venkatesh, D. N., Durazzo, A., Lucarini, M., Eder, P., Silva, A. M., Santini, A., & Souto, E. B. (2020). Polymeric nanoparticles: Production, characterization, toxicology and ecotoxicology. Molecules, 25(16), 3731. https://doi.org/10.3390/molecules25163731

Zhang, H., Oh, M., Allen, C., & Kumacheva, E. (2004). Monodisperse chitosan nanoparticles for Mucosal Drug Delivery. Biomacromolecules, 5(6), 2461–2468. https://doi.org/10.1021/bm0496211

Declaration of interests

☒ The authors declare that they have no known competing financial interests or personal relationships that could have appeared to influence the work reported in this paper.

☐The authors declare the following financial interests/personal relationships which may be considered as potential competing interests:

Authorship Contribution

Giorgia Maurizii: Conceptualization, Methodology, Data curation, Investigation, Formal Analysis, Validation, Writing original draft.

Sofia Moroni: Investigation, methodology, Validation, Review & editing.

Javier Vincente Jimènez Núnez: Conceptualization, Investigation, Validation, Review & editing

Giulia Curzi: Investigation, validation, Visualization, Review & editing

Mattia Tiboni: Conceptualization, Methodology, Validation, Visualization, Review & editing.

Annalisa Aluigi: Conceptualization, Methodology, Data curation, Formal Analysis, Visualization, Writing original draft.

Luca Casettari: Conceptualization, Data curation, Project administration, Supervision, Review & editing, Project administration.